Length scale of a chaotic element in Rayleigh-Bénard convection

A. Karimi
Department of Engineering Science and Mechanics, Virginia Polytechnic Institute and State University, Blacksburg, Virginia 24061, USA

M. R. Paul
Department of Mechanical Engineering, Virginia Polytechnic Institute and State University, Blacksburg, Virginia 24061, USA

(Received 21 May 2012; published 20 December 2012)

We describe an approach to quantify the length scale of a chaotic element of a Rayleigh-Bénard convection layer exhibiting spatiotemporal chaos. The length scale of a chaotic element is determined by simultaneously evolving the dynamics of two convection layers with a unidirectional coupling that involves only the time-varying values of the fluid velocity and temperature on the lateral boundaries of the domain. In our results we numerically simulate the full Boussinesq equations for the precise conditions of experiment. By varying the size of the boundary used for the coupling we identify a length scale that describes the size of a chaotic element. The length scale of the chaotic element is of the same order of magnitude, and exhibits similar trends, as the natural chaotic length scale that is based upon the fractal dimension.

DOI: 10.1103/PhysRevE.86.066212 PACS number(s): 05.45.Jn, 05.45.Pq, 05.45.Xt, 47.20.Bp

I. INTRODUCTION

Despite intense theoretical and experimental investigation many open questions remain in our understanding of the dynamics of spatially extended systems that are driven far from equilibrium [1]. Important examples include the dynamics of the atmosphere, oceans, and climate; fluid turbulence; and the dynamics of reacting-diffusing-advecting systems. A common feature of these systems is spatiotemporal chaos where the dynamics are aperiodic in space and time. Significant progress has been made in understanding chaos in time using dynamical systems theory and chaotic time series analysis. However, a similar depth of understanding of spatiotemporal chaos is lacking. A question of particular interest is the identification of appropriate length scales that describe and provide insight into spatiotemporal chaos [2–7].

We explore these questions using the canonical pattern forming system of Rayleigh-Bénard convection that results when a shallow layer of fluid is heated uniformly from below in a gravitational field [1]. For experimentally accessible continuous systems, such as fluid convection, the dimension of the attractor describing the dynamics is expected to be very large [8–10]. Using modern algorithms and supercomputing resources it is now possible to compute the fractal dimension of such systems for the precise conditions of experiment (cf. [10]). This has led to a number of new insights yet many important questions remain. For example, given knowledge of the fractal dimension one can estimate a time average of the size of a chaotic degree of freedom or chaotic element [11]. For typical conditions of the spiral defect chaos state in Rayleigh-Bénard convection [12] this length scale is of the order of the wavelength of the pattern [8–10] which is also consistent with the approximate size of the defects in the pattern. However, it has been very difficult to find a quantitative link between the chaotic length scale and a diagnostic based upon the dynamics of the pattern such as the time variation of the fluid velocity or temperature field [3,5,8,10].

Insights into the underlying length scales that describe spatiotemporal chaos have been gained by studying the synchronization of systems exhibiting spatiotemporal chaos [13–16]. Relevant to our work is the fluid study on the synchronization of coupled rotating baroclinic annuli which is important for understanding long-range connections in atmospheric dynamics [17]. In this paper we appeal to ideas from synchronization to gain new insights into the fundamental composition of high-dimensional spatiotemporal chaos. We quantify the spatial extent required to support nearly identical dynamics between the two convection layers and explore how this length scale relates to the chaotic length scale determined from the fractal dimension.

II. APPROACH

The nondimensional Boussinesq equations that govern Rayleigh-Bénard convection are

$$\partial_t \mathbf{u} + (\mathbf{u}\cdot\boldsymbol{\nabla})\,\mathbf{u} = -\boldsymbol{\nabla} p + \sigma R T \hat{\mathbf{z}} + \sigma \nabla^2 \mathbf{u}, \tag{1}$$

$$\partial_t T + (\mathbf{u}\cdot\boldsymbol{\nabla})\,T = \nabla^2 T, \tag{2}$$

$$\boldsymbol{\nabla}\cdot\mathbf{u} = 0, \tag{3}$$

where $\mathbf{u}$ is the fluid velocity, T is the temperature, p is the pressure, and $\hat{\mathbf{z}}$ is a unit vector opposing gravity. We have used the standard convention where the layer depth d is the length scale, the constant temperature difference between the top and bottom plates is the temperature scale, and the vertical diffusion time for heat is the time scale. The nondimensional parameters are the Rayleigh number R, the Prandtl number σ, and the aspect ratio $\Gamma = L/d$ where L is the side length of the square domain.

Our basic approach for determining the length scale of a chaotic element is illustrated in Fig. 1. This approach has been used to study the length scales of a two-dimensional array of coupled map lattices [18]. Consider a large principal domain with a box geometry and aspect ratio Γ_p where the system parameters yield chaotic convection. Now consider a second convection layer with a smaller aspect ratio Γ_t which we refer to as the target domain. The target domain receives its time-dependent lateral sidewall boundary conditions for the fluid

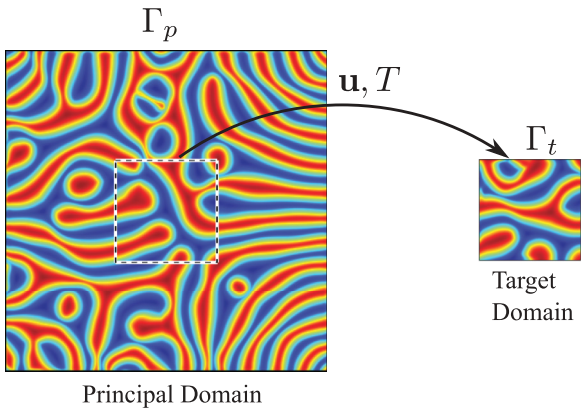

FIG. 1. (Color online) A principal domain with an aspect ratio $\Gamma_p = 32$ (left) and a target domain with an aspect ratio $\Gamma_t = 10$ (right). The subdomain is within the principal domain and is indicated by the dashed box. Color contours are of the temperature field at the horizontal midplane where red (light gray) is hot rising fluid and blue (dark gray) is cool falling fluid. The time-dependent values of the velocity and temperature fields on the lateral boundary of the subdomain are used as boundary conditions on the target domain and are indicated by the arrow. The principal and target domains begin from different random initial conditions. For the case shown ($\epsilon = 2.51, \sigma = 1$) the dynamics are not similar since $\Gamma_t > \xi_c$.

velocity and temperature from the dashed boundary illustrated within the principal domain which we call the subdomain.

It is useful to highlight an important distinction between the subdomain and the target domain. The subdomain is embedded within the principal domain. The target domain, on the other hand, is not embedded within a larger domain and only receives time-dependent boundary conditions for the velocity and temperature from the subdomain. For incompressible fluid dynamics the pressure is not an independent dynamical variable and is determined implicitly to satisfy the conservation of mass for the entire domain. In light of this, the fluid pressure at the boundary is not passed from the subdomain to the target domain. The pressure in the target domain, including the values of the pressure at the lateral boundaries, is determined at every time step when enforcing the incompressibility of the fluid. The pressure in the subdomain is determined when enforcing incompressibility for the entire principal domain. As a result, the pressure field for the subdomain and the target domain will be different even when the fluid patterns of the subdomain and target domain appear to be similar.

Overall, there is a unidirectional flow of information from the subdomain to the target domain. We emphasize that the entire sidewall boundary is used whereas Fig. 1 only shows the midplane slice. The principal and target domains start from different random initial conditions in the temperature field. Both convection layers are integrated simultaneously and the dynamics of the subdomain and target domain are compared.

The similarity of the dynamics depends upon the aspect ratio of the target domain and therefore the subdomain since $\Gamma_t = \Gamma_{\rm sd}$ in all of our results where $\Gamma_{\rm sd}$ is the aspect ratio of the subdomain. For $\Gamma_t \ll 1$ it is expected that the dynamics of the two convection layers will become identical. Similarly, for $\Gamma_t \gg 1$ the dynamics of the two chaotic layers should be uncorrelated. We are interested in finding the largest value of Γ_t that will support dynamics that are nearly identical. We call the side length of the largest target domain the chaotic element length scale ξ_c. Furthermore, we want to quantify how this length scale varies with the Rayleigh number and how its magnitude compares with the chaotic length scale determined from the fractal dimension.

III. RESULTS AND DISCUSSION

For our calculations we have numerically integrated two copies of Eqs. (1)–(3) (one copy for each convection layer) that include the unidirectional coupling from the subdomain to the target domain using the approach described by Chiam *et al.* [19] (see also [20]). We have used a uniform spatial resolution of $\Delta = 1/8$ and a time step of $\Delta t = 0.001$. We have performed numerous tests including spatial and temporal resolution tests as well as running simulations from numerous random initial conditions to ensure the validity and generality of our calculations.

We have found that a good diagnostic for the determination of ξ_c is to use the difference in the Nusselt number between the two convection layers $\Delta N = N_{\rm sd} - N_t$ where $N_{\rm sd}$ and N_t are the Nusselt numbers for the subdomain and target domain, respectively. Significant advantages of using the Nusselt number are its experimental accessibility and the fact that a single number can be used to compare the three-dimensional states of two convection layers at any time. Although the Nusselt number is a global measure of the heat transport through the fluid layer, its variation in time directly reflects the pattern dynamics (cf. [10,21]). The presence of a defect hinders the heat transport through the layer causing a dip in the Nusselt number, the annihilation of a defect improves the heat transport resulting in a spike in the Nusselt number, and glide and climb dynamics result in a meandering of $N(t)$. The defect events can be very rapid, $t \ll 1$, and can result in sharp features of the time variation of the Nusselt number. We have also computed ξ_c using the difference between the complete states of the two convection layers and have found the same trends.

Even for two chaotic convection layers exhibiting dynamics that are indistinguishable to the eye there is some variation between the target and subdomain states and, as a result, they are not identical or synchronized. These small variations occur spatially near the regions of rapid birth and annihilation of defect structures. This variation is captured in $\Delta N(t)$ near the sharp features of the Nusselt number and results in large rapid spikes in the time series of ΔN. We anticipate that these deviations are due to the nonlocal dynamics of a weak mean flow that is present (cf. [1,22–24]). The mean flow is a long-range flow due to wave number gradients, amplitude gradients, and roll curvature that acts over length scales larger than the roll wavelength and is well known to affect the stability of convection rolls. Due to the nonlocal nature of the mean flow it will be different for the subdomain and target domain since the target domain is only passed the boundary information and the subdomain dynamics are affected by the mean flow generated by the surrounding convection pattern. We have not explored this aspect in detail and emphasize that the deviations observed are quite small.

In order to not include these rapid and sharp features of ΔN in our criterion for ξ_c we first low-pass filter $N(t)$ to remove

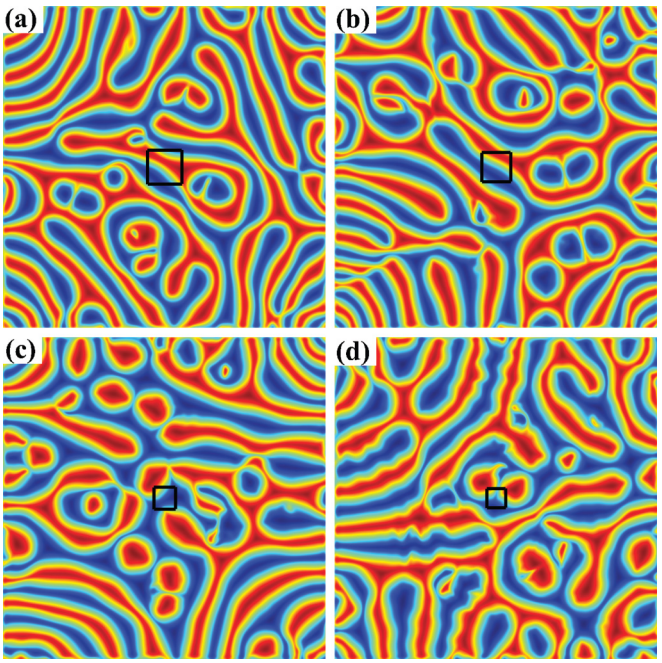

FIG. 2. (Color online) The chaotic element length scale ξ_c for a range of reduced Rayleigh numbers ϵ for a principal domain with $\Gamma_p = 32$. The color contours are of the temperature field. The black box inside the principal domain has a side length of ξ_c. (a) $\epsilon = 2.51$, $\xi_c = 3.4$; (b) $\epsilon = 3.1$, $\xi_c = 2.9$; (c) $\epsilon = 3.68$, $\xi_c = 2.1$; and (d) $\epsilon = 4.27$, $\xi_c = 1.9$.

dynamics from ΔN that occur at frequencies $f_0 \gtrsim 3.3$ before checking the dynamics. This corresponds to dynamics for $t \lesssim 0.3$ whereas the time scale describing the overall dynamics of the convection rolls is $t \approx 1$. The value of ξ_c is nearly independent (less than one percent deviation) of the particular choice of f_0 over the wide range $2.5 \lesssim f_0 \lesssim 5$.

We have chosen to explore parameters that yield the state of spiral defect chaos in large convection layers [12] which is anticipated to be extensively chaotic [8,9]. To achieve this we have used a box geometry with $\Gamma_p = 32$ and a fluid with a Prandtl number of $\sigma = 1$. We anticipate that our results are independent of Γ_p as long as the system size is large enough to be extensive. Flow field images are shown in Fig. 2 as temperature contours at the horizontal midplane. The different panels are for different values of the reduced Rayleigh number ϵ where $\epsilon = (R - R_c)/R_c$ and $R_c \simeq 1708$ is the critical value. The value of ϵ is increasing from (a) to (d) and the small black box in the center of each domain has a side length of ξ_c. We have determined the precise value of ξ_c by running many numerical simulations for different values of Γ_t. It is clear from the Fig. 2 that ξ_c decreases with increasing ϵ.

Figure 3 illustrates the time variation of the Nusselt number difference between the target and subdomain for the chaotic dynamics shown in Fig. 2(a) where $\xi_c = 3.4$. In panel (a) the aspect ratio of the target domain is $\Gamma_t = 2$ and the dynamics are nearly identical where $|\Delta N| \lesssim 5 \times 10^{-3}$ for the duration of the simulation (3000 time units are shown). Panel (b) shows results for $\Gamma_t = 10$ that yields chaotic dynamics that are not similar where $|\Delta N| \lesssim 0.1$.

Figure 4 illustrates the variation of the maximum value of $|\Delta N|$ over a range of target domain sizes $2 \leqslant \Gamma_t \leqslant 8$

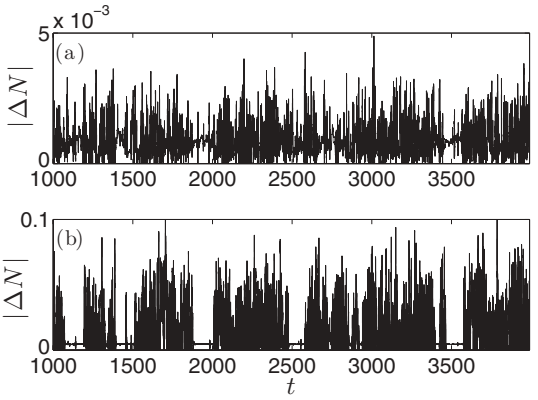

FIG. 3. The time variation of $|\Delta N|$ for chaotic dynamics for $\Gamma_p = 32$, $\epsilon = 2.51$, and $\sigma = 1$. (a) $\Gamma_t = 2$ yields nearly identical dynamics. (b) $\Gamma_t = 10$ does not yield similar dynamics.

for $\epsilon = 2.51$ and $\sigma = 1$. The circles are results for $\Gamma_p = 32$ which yields chaotic dynamics. The line is included to guide the eye and the dashed horizontal line at $|\Delta N| = 0.01$ is our threshold for determining ξ_c. The magnitude of $|\Delta N|$ decreases rapidly with decreasing target domain sizes. Using our approach the two convection layers are nearly identical for $\Gamma_t \lesssim 3.4$ and therefore $\xi_c = 3.4$. We point out that for $\Gamma_t < \xi_c$ the magnitude of $|\Delta N|$ does not change significantly. Similar trends were observed for our numerical results at different values of ϵ. The squares in Fig. 4 are for a smaller sized principal domain where $\Gamma_p = 16$ with $\epsilon = 2.51$ and $\sigma = 1$ which yielded time-periodic dynamics of the flow field. In this case, the dynamics of the target domain was nearly identical to that of the subdomain for all sizes of the target domain.

It is insightful to compare quantitatively the chaotic element length scale and other important length scales in the problem. Figure 5 illustrates the variation of the pattern wavelength

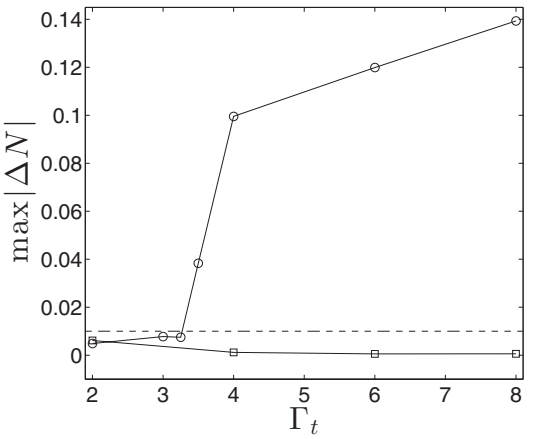

FIG. 4. Variation of the maximum value of $|\Delta N|$ over a range of target domain aspect ratios Γ_t for $\sigma = 1$ and $\epsilon = 2.51$. Squares are for $\Gamma_p = 16$ which yields time-periodic dynamics where dynamics of the target domain and subdomain were nearly identical for all Γ_t. Circles are for $\Gamma_p = 32$ which yields chaotic dynamics (pattern images are shown in Fig. 2). The threshold of $|\Delta N| \leqslant 0.01$ is indicated by the dashed line. The chaotic element length scale for the chaotic dynamics is $\xi_c = 3.4$. The solid lines are included to guide the eye.

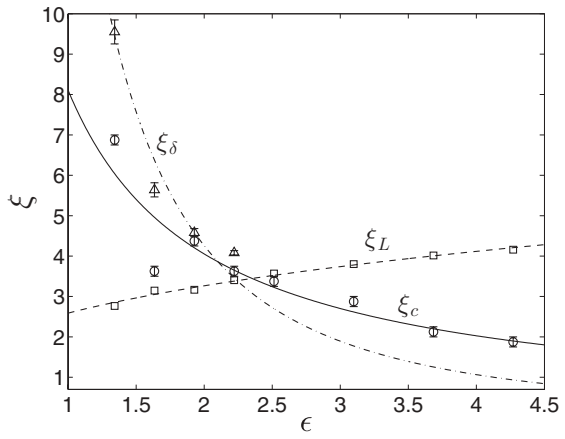

FIG. 5. Variation of the chaotic element length scale ξ_c (circles), the natural chaotic length scale ξ_δ (triangles), and the pattern wavelength ξ_L (squares) with the reduced Rayleigh number ϵ for a principal domain with an aspect ratio of $\Gamma_p = 32$. The dashed line is $\xi_L = 2.6\epsilon^{0.33}$, the solid line is $\xi_c = 8.1\epsilon^{-1}$, and the dash-dotted line is $\xi_\delta = 17.0\epsilon^{-2}$. Error bars are included for ξ_c and ξ_δ.

ξ_L, the chaotic length scale ξ_δ, and ξ_c over a range of reduced Rayleigh numbers $1 \lesssim \epsilon \lesssim 4.5$. Squares are the time-averaged value of the pattern wavelength determined using the structure factor [1]. Over the range shown the pattern wavelength increases slightly and the dashed line is a curve fit through the data of the form $\xi_L = 2.6\epsilon^{0.33}$. Circles are ξ_c which decreases with increasing ϵ and the solid line is a power-law curve fit of the form $\xi_c = 8.1\epsilon^{-1}$. The error bars shown for ξ_c reflect the precision in terms of the discretization used in determining the largest Γ_t yielding ξ_c. This could be improved by performing more simulations for different values of Γ_t.

The natural chaotic length scale ξ_δ is computed from the fractal dimension D_λ. To compute D_λ we have simultaneously integrated many copies of the tangent space equations (cf. [8,10]) and used the standard approach of frequent Gram-Schmidt reorthonormalizations to compute the spectrum of Lyapunov exponents. For these computations we used a highly efficient, parallel, and spectral element solver that is discussed in detail elsewhere [10,22]. Given the spectrum of Lyapunov exponents the fractal dimension is $D_\lambda = K + S_K/|\lambda_{K+1}|$ where K is the largest n for which $S_n = \sum_{i=1}^{n} \lambda_i > 0$ [1]. A volume of size $\xi_\delta^{d_s}$ contains a single chaotic degree of freedom on average [11] where $\xi_\delta = (D_\lambda/\Gamma^{d_s})^{-1/d_s}$ and d_s is the number of spatially extended dimensions (where $d_s = 2$ for large shallow convection layers) [1]. In order to compute D_λ, and therefore ξ_δ, one must compute enough Lyapunov exponents such that their linearly interpolated sum equals zero. For chaotic Rayleigh-Bénard convection in large domains this is a large number requiring significant computing resources [10]. The expense of these calculations has limited the range in ϵ for which we present values of ξ_δ. For our calculations, $D_\lambda \approx 11$ for $\epsilon = 1.34$ and $D_\lambda \approx 61$ for $\epsilon = 2.22$. Our results for ξ_δ are shown as triangles in Fig. 5 where the dash-dotted line is the power-law curve fit $\xi_\delta = 17\epsilon^{-2}$. We have included error bars on ξ_δ that reflect its standard deviation in time.

Although the pattern wavelength is increasing with increasing ϵ, both ξ_c and ξ_δ exhibit similar trends and are of the same order of magnitude. Therefore the length scale of a chaotic element is on the order of the chaotic length scale determined from the fractal dimension. These results support the idea that it may be possible to decompose a spatiotemporally chaotic flow field into spatial elements that contain a single chaotic degree of freedom on average.

IV. CONCLUSION

In conclusion, we have quantified the length scale of a chaotic element by coupling the dynamics of two convection layers using only information passed unidirectionally to the boundary of the target domain. We have used this to show that ξ_c is of the same order of magnitude and exhibits similar trends as the computationally intensive chaotic length scale ξ_δ. Although the connection between the two is not rigorous our results suggest that there is a length scale associated with the pattern dynamics that can be linked with the chaotic length scale. This provides an avenue of investigation that does not require the expensive computation of the Lyapunov spectra. It may be possible to investigate experimentally these ideas using time-dependent boundary conditions and it would be interesting to explore the robustness of our results in situations accessible to experiment.

ACKNOWLEDGMENTS

This research was supported by NSF Grant No. CBET-0747727. We are grateful for use of the Advanced Research Computing center at Virginia Tech. We have had many fruitful discussions with Mike Cross, Katie Richardson, Paul Fischer, and Keng-Hwee Chiam.

[1] M. C. Cross and P. C. Hohenberg, Rev. Mod. Phys. **65**, 851 (1993).
[2] M. P. Fishman and D. A. Egolf, Phys. Rev. Lett. **96**, 054103 (2006).
[3] C. S. O'Hern, D. A. Egolf, and H. S. Greenside, Phys. Rev. E **53**, 3374 (1996).
[4] S. Tajima and H. S. Greenside, Phys. Rev. E **66**, 017205 (2002).
[5] D. A. Egolf and H. S. Greenside, Nature (London) **369**, 129 (1994).
[6] A. Karimi and M. R. Paul, Chaos **20**, 043105 (2010).
[7] D. Stahlke and R. Wackerbauer, Phys. Rev. E **83**, 046204 (2011).
[8] D. A. Egolf, I. V. Melnikov, W. Pesch, and R. E. Ecke, Nature (London) **404**, 733 (2000).
[9] M. R. Paul, M. I. Einarsson, P. F. Fischer, and M. C. Cross, Phys. Rev. E **75**, 045203 (2007).
[10] A. Karimi and M. R. Paul, Phys. Rev. E **85**, 046201 (2012).
[11] J. D. Farmer, E. Ott, and J. A. Yorke, Physica D **7**, 153 (1983).
[12] S. W. Morris, E. Bodenschatz, D. S. Cannell, and G. Ahlers, Physica D **97**, 164 (1996).

[13] S. Boccaletti, J. Bragard, and F. T. Arecchi, Phys. Rev. E **59**, 6574 (1999).
[14] A. Pikovsky, M. Rosenblum, and J. Kurths, *Synchronization: A Universal Concept in Nonlinear Science* (Cambridge University Press, Cambridge, 2001).
[15] G. Hu, J. H. Xiao, J. Z. Yang, F. G. Xie, and Z. L. Qu, Phys. Rev. E **56**, 2738 (1997).
[16] L. Kocarev, Z. Tasev, and U. Parlitz, Phys. Rev. Lett. **79**, 51 (1997).
[17] A. A. Castréjon-Pita and P. L. Read, Phys. Rev. Lett. **104**, 204501 (2010).
[18] K. Richardson and M. C. Cross, Caltech Summer Undergraduate Research Program, 2004 (unpublished).
[19] K.-H. Chiam, M. C. Lai, and H. S. Greenside, Phys. Rev. E **68**, 026705 (2003).
[20] A. Karimi, Ph.D. thesis, Virginia Polytechnic Institute and State University, 2012.
[21] M. R. Paul, M. C. Cross, P. F. Fischer, and H. S. Greenside, Phys. Rev. Lett. **87**, 154501 (2001).
[22] M. R. Paul, K.-H. Chiam, M. C. Cross, P. F. Fischer, and H. S. Greenside, Physica D **184**, 114 (2003).
[23] K.-H. Chiam, M. R. Paul, M. C. Cross, and H. S. Greenside, Phys. Rev. E **67**, 056206 (2003).
[24] A. C. Newell, T. Passot, and M. Souli, J. Fluid Mech. **220**, 187 (1990).